Temperature Modelling of the Biomass Pretreatment Process

Prunescu, Remus Mihail; Blanke, Mogens; Jensen, Jakob M.; Sin, Gürkan

Published in:
Proceedings of the 17th Nordic Process Control Workshop

Publication date:
2012

Document Version
Publisher's PDF, also known as Version of record

Proceedings of the 17th Nordic Process Control Workshop
Technical University of Denmark, Kgs Lyngby, Denmark
January 25-27, 2012

Temperature Modelling of the Biomass Pretreatment Process

Remus M. Prunescu * **Mogens Blanke** ** **Jakob M. Jensen** ***
Gürkan Sin ****

* *DONG Energy A/S, Innovationscenter, Nesa Allé 1, DK 2820 Gentofte, Denmark (e-mail: rempr@dongenergy.dk)*
** *Department of Electrical Engineering, Automation and Control Group, Technical University of Denmark, Elektrovej, Build. 326, DK 2800 Kgs. Lyngby, Denmark (e-mail: mb@elektro.dtu.dk)*
*** *DONG Energy A/S, Power Concept Optimisation, Nesa Allé 1, DK 2820 Gentofte, Denmark (e-mail: jammu@dongenergy.dk)*
**** *Department of Chemical and Biochemical Engineering, CAPEC, Sølvtofts Plads, Build. 227, Technical University of Denmark (e-mail: gsi@kt.dtu.dk)*

Abstract: In a second generation biorefinery, the biomass pretreatment stage has an important contribution to the efficiency of the downstream processing units involved in biofuel production. Most of the pretreatment process occurs in a large pressurized thermal reactor that presents an irregular temperature distribution. Therefore, an accurate temperature model is critical for observing the biomass pretreatment. More than that, the biomass is also pushed with a constant horizontal speed along the reactor in order to ensure a continuous throughput. The goal of this paper is to derive a temperature model that captures the environmental temperature differences inside the reactor using distributed parameters. A Kalman filter is then added to account for any missing dynamics and the overall model is embedded into a temperature soft sensor. The operator of the plant will be able to observe the temperature in any point of the thermal reactor. Real data sets were extracted from the Inbicon biorefinery situated in Kalundborg, Denmark, and will be utilized to validate and test the temperature model.

Keywords: dynamic modelling, computational fluid dynamics, bioethanol, biomass pretreatment, thermal reactor, biorefinery, Inbicon

1. INTRODUCTION

The worldwide economy is nowadays based on fossil fuels like coal, petroleum and natural gases, which have become increasingly more demanded and difficult to obtain as the current deposits are getting closer to depletion. Fossil fuels are also responsible for most of the climate changes humanity is facing and alternatives to such energy sources receive increasingly more interest. Bioethanol is thought to become the primary renewable liquid fuel (Datta et al., 2011) and solutions to its large scale production from agricultural wastes are intensively investigated.

In this context, DONG Energy built a bioethanol demonstration plant in 2009 at Kalundborg, Denmark, in order to prove that second generation technology of conversion of lignocellulosic biomass waste into ethanol can be profitably applied on a large scale. The conception principle of the plant is the Integrated Biomass Utilization System (IBUS) developed by DONG Energy, which is based on a symbiosis between a biorefinery and a power plant. The IBUS process is commercially exploited by Inbicon A/S, the biomass refinery division of DONG Energy. A detailed description of the refinery process has been documented by Larsen et al. (2008) and is graphically represented in figure 1. The production cycle starts with the pretreatment stage, necessary to break down the biomass into smaller fibres in order to facilitate the subsequent enzymatic digestibility. The pretreatment step is based only on steam from the power plant and recycled water. The next step is the enzymatic liquefaction of the pretreated fibre fraction characterized by a high dry matter content. The resulted slurry is sent to the fermentation tank and is followed by the distillation subprocess. Lignin is recovered as bio-pallets and is utilized as solid fuel in the power plant. Another by-product of the biorefinery is the C5 molasses, a syrup high in nutritional value for livestock.

The successfulness of biomass conversion to ethanol highly depends on the pretreatment stage, which is also responsible for the appearance of inhibitors that affect the enzymatic digestibility (Thomsen et al., 2009). Modelling endeavours have been conducted by Petersen et al. (2009) in order to determine optimal parameters of the pretreatment process. According to (Overend et al., 1987), the pretreatment stage can be characterized by two parameters i.e. the retention time and the steam temperature. These parameters were gathered in a single indicator called the severity factor. Petersen et al. (2009) succeeded in finding a relation between the severity factor and the chemical composition of the slurry that enters the enzymatic treatment stage

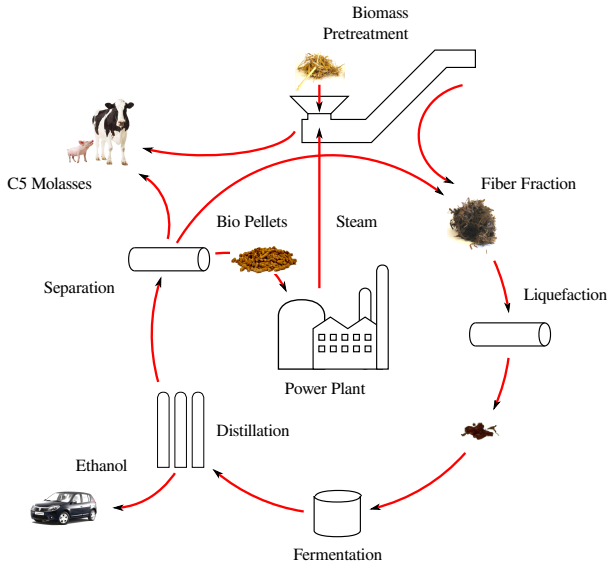

Fig. 1. The IBUS Process (Larsen et al., 2008).

thus offering an estimate of the conversion of biomass to ethanol.

One of the drawbacks of the severity factor developed by Overend et al. (1987) is the fact that it assumes a uniform environment with constant temperature. Therefore, the goal of this article is to find a more accurate mathematical model of the temperature given an irregular moving environment. Knowledge from computational fluid dynamics will be applied in order to account these spatial temperature differences. To simplify simulations, the model is serialized and expressed in a standard state space formulation. In the end, a Kalman filter is added and the overall model will be embedded into a temperature soft sensor that allows the operator to observe how the biomass is treated in any point of the reactor.

2. DESCRIPTION OF THE BIOMASS PRETREATMENT PROCESS

Kristensen et al. (2008) investigated the effects of various pretreatment processes on biomass and his results show that cellulose is not degraded in the hydrothermal pretreatment process but rather becomes more accessible to enzymes due to relocation of lignin and substantial removal of hemicellulose.

The main component of the Inbicon pretreatment process is a pressurized thermal reactor presented in figure 2. Soaked biomass is released from a pressurization unit every 2 min through the left inlet of the tank and, with the help of a motorized snail, the biomass is pushed horizontally with a constant speed till the outlet. The optimal values of the retention time i.e. 15 min and of the reactor temperature i.e. 195 °C($\approx$ 13 bar) were determined based on the experiments of Petersen et al. (2009). The horizontal speed is set to a constant value in order to meet the retention time constraint. The optimal temperature is ensured by a pressure control system that injects saturated steam from the bottom of the reactor through several inlets.

Two temperature measurement belts of 5 sensors each are installed at the beginning and at the end of the tank. The

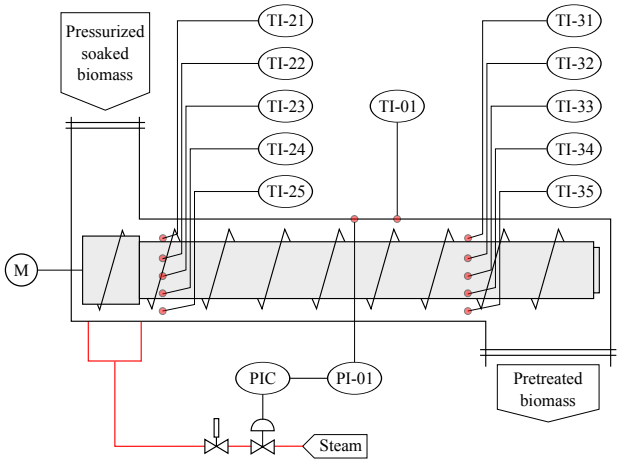

Fig. 2. The thermal reactor schematic diagram with instrumentation.

labels of the temperature sensors, enumerated from top to bottom, are TI-21, TI-22, TI-23, TI-24 and TI-25 for the left group and, respectively, TI-31, TI-32, TI-33, TI-34 and TI-35 for the right series. The reactor pressure is measured by PI-01 and the pressure controller is notated as PIC. A layer of steam is formed in the top part of the reactor as the tank is not fully filled with biomass and its temperature is monitored by TI-01.

3. MATHEMATICAL MODELLING OF THE THERMAL REACTOR

3.1 Preliminary Analysis

The purpose of the thermal reactor modelling is to obtain a temperature gradient that accurately describes the temperature distribution inside the reactor in a two dimensional space. The temperature variations along the width of the reactor are neglected due to its reduced length. Figure 3 contains temperature sensor data that was logged during a nominal operational mode of the plant.

Figure 3 presents temperature variations inside the reactor both on horizontal and vertical axes. A preliminary analysis of the temperature measurements illustrates that the temperature is not uniform but it rather varies considerably mainly on vertical. A difference of about $10 - 15\,^{\circ}\mathrm{C}$ is recorded between the top and the bottom parts of the reactor. The right end of the reactor is open to another subcomponent of the process and it is responsible for a temperature drop on horizontal as the outlet is approached. It is hard to properly model the energy loss due to the open end of the reactor and a Kalman filter will be implemented to account for these effects.

3.2 Temperature Modelling

In order to describe the thermal effects accurately both in space and time, partial differential equations are needed. Computational fluid dynamics collects the tools and methods for describing the heat diffusion in a moving environment such as the heat convection diffusion equation (Egeland and Gravdahl, 2002):

$$\frac{\partial\left(\rho c T\right)}{\partial t} + \nabla^{\mathrm{T}}\left(\rho c \mathbf{u} T\right) = \nabla^{\mathrm{T}}\left(\Gamma c \nabla T\right) + S_T \qquad (1)$$

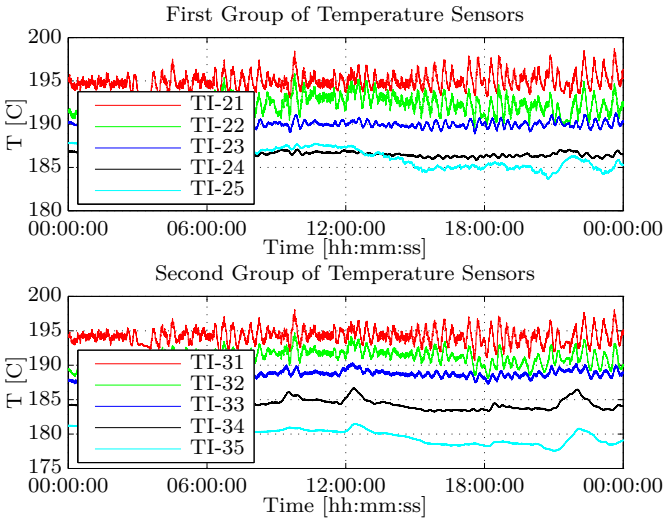

Fig. 3. Preliminary analysis of the temperature inside the reactor. The top subplot contains the temperature recorded by the sensors from the beginning of the reactor while the bottom subplot describes the temperature at the right end of the tank.

where the first term on the left hand side of the equation is the rate of change of temperature T in a fluid element, the second term on the left hand side is the temperature loss due to convection, the first term on the right side is the rate of change due to heat diffusion and the last term is the change caused by the heat source S_T. The density of the material is denoted as ρ, c is the specific heat, $\mathbf{u}$ is the velocity vector and Γ is the diffusion coefficient. The product between the diffusion coefficient Γ and the specific heat c is notated as κ and is called the thermal conductivity of the material:

$$\kappa = \Gamma c \tag{2}$$

In two dimensions, equation (1) can be explicitly written as:

$$\begin{aligned} \rho c\frac{\partial T}{\partial t} + \rho c\frac{\partial\left(\mathbf{u}T\right)}{\partial x} + \rho c\frac{\partial\left(\mathbf{u}T\right)}{\partial y} = \\ = \frac{\partial}{\partial x}\left(\kappa\frac{\partial T}{\partial x}\right) + \frac{\partial}{\partial y}\left(\kappa\frac{\partial T}{\partial y}\right) + S_T \end{aligned} \tag{3}$$

where ρ, c and κ are considered constant. The slurry is pushed horizontally with a constant speed and, therefore, the velocity vector $\mathbf{u}$ has a single constant component u_x on the x axes:

$$\mathbf{u} = \begin{bmatrix} u_x & 0 & 0 \end{bmatrix}^{\mathrm{T}} \tag{4}$$

Any other mixture effects that might occur due to the movement are neglected. Equation (3) is then rewritten considering the movement on a single axes:

$$\rho c\frac{\partial T}{\partial t} + \rho c u_x\frac{\partial T}{\partial x} = \frac{\partial}{\partial x}\left(\kappa\frac{\partial T}{\partial x}\right) + \frac{\partial}{\partial y}\left(\kappa\frac{\partial T}{\partial y}\right) + S_T \tag{5}$$

Equation (5) is parabolic in time and the finite volume method is a way to solve it (Egeland and Gravdahl, 2002). The first step in the finite volume method is to break down the two dimensional space into control volumes or in a grid as in figure 4 where only one central control volume P and its neighbours north N, south S, east E and west W are shown. The central points of the neighbours are denoted with capital letters while the boundaries are notated as north n, south s, east e and west w. The distance from the west w to the east e boundaries is δx_{we} and represents the width of the control volume. The distance from the north n to the south s boundaries is shown as δx_{ns} and is also called the height of the control volume. In order to simplify calculations it is convenient to choose square control volumes i.e. $\delta x_{we} = \delta x_{ns} = \Delta x$.

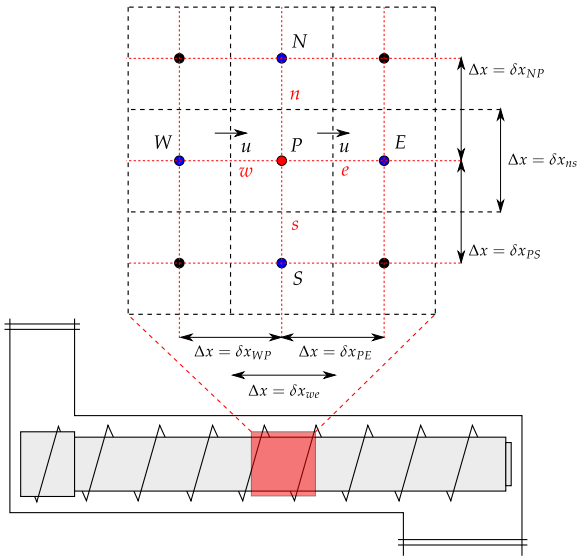

Fig. 4. A control volume with its neighbours from a two dimensional grid.

The Finite Volume Method The solving procedure of equation (5) including its discretization has been moved to appendix A.1 and A.2. The following solution was determined:

$$\begin{aligned} a_P^{n+1}T_P^{n+1} &= a_P^nT_P^n + a_E^nT_E^n + a_W^nT_W^n + a_S^nT_S^n + a_N^nT_N^n + \\ &+ a_E^{n+1}T_E^{n+1} + a_W^{n+1}T_W^{n+1} + a_S^{n+1}T_S^{n+1} + \\ &+ a_N^{n+1}T_N^{n+1} + S_u \end{aligned} \tag{6}$$

with coefficients a_P^n, a_E^n, a_W^n, a_S^n, a_N^n and a_P^{n+1}, a_E^{n+1}, a_W^{n+1}, a_S^{n+1}, a_N^{n+1}:

$$\begin{aligned} a_P^n &= \rho c\frac{\Delta V}{\Delta t} - \theta\left(4D + F\right) \\ a_E^n &= \theta D \\ a_W^n &= \theta\left(D + F\right) \\ a_S^n &= \theta D \\ a_N^n &= \theta D \\ a_P^{n+1} &= \rho c\frac{\Delta V}{\Delta t} + \left(1-\theta\right)\left(4D + F\right) \\ a_E^{n+1} &= \left(1-\theta\right)D \\ a_W^{n+1} &= \left(1-\theta\right)\left(D + F\right) \\ a_S^{n+1} &= \left(1-\theta\right)D \\ a_N^{n+1} &= \left(1-\theta\right)D \end{aligned} \tag{7}$$

where θ is the integration method parameter, D is the diffusion term, F is the convection term, ΔV is the volume of the control object and Δt is the integration step. The integration parameter θ can be 0, 1 or 0.5 corresponding to an implicit Euler, explicit Euler or Crank-Nicholson solver.

A Crank-Nicholson solver is preferred due to its accuracy. Coefficients F and D were explicitly identified as below in appendix A.2:

$$\begin{aligned} F &= \rho c u_x A \\ D &= \frac{\kappa A}{\Delta x} \end{aligned} \tag{8}$$

where A is the side area of the control volume. Because the physical changes of the material along the reactor are neglected i.e. ρ and κ remain constant in any point of the reactor, the diffusion coefficient D becomes also constant regardless of the boundary. If the horizontal speed u_x is held constant then the convection coefficient F becomes constant. If the physical parameters of the biomass change or the horizontal speed is modified then D and F must be updated every simulation step.

The control volumes situated near the borders do not have certain neighbours and are treated differently. The changes that occur in the coefficients are also referred to as the boundary conditions.

Boundary Conditions The boundary conditions are set as suggested by (Bingham et al., 2010). There are two types of boundary conditions depending on whether the temperature is considered known (Dirichlet condition) or the temperature gradient or energy loss is estimated at the border (Neumann type). Figure 5 illustrates the Dirichlet and Neumann setup for a general grid where the boundary condition is notated as T_i or D_i where i is one of the borders i.e. east e, west w, south s or north n.

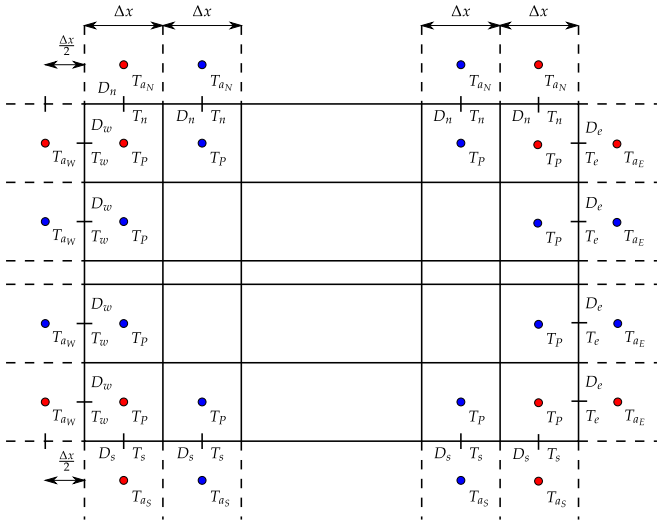

Fig. 5. Dirichlet and Neumann boundary conditions. Dirichlet boundary conditions are denoted as T_i where i is the boundary while Neumann conditions are notated as D_i.

The boundary conditions reflect in several changes of the model coefficients corresponding to the border control volumes. The entire derivation procedure of the coefficients update can be found in appendix A.3. Briefly, a virtual neighbour is created and equation (6) is rewritten considering the extra neighbour.

The reactor is only partially filled with biomass, so the top temperature sensor i.e. TI-01 actually measures the temperature of a steam layer. This measurement constitutes one of the borders and its value is considered the same along the x axes due to the layer of steam. This is a Dirichlet condition and the model coefficients of the northern control volumes change as below:

$$\begin{aligned} \underbrace{(a_P^{n+1} + a_N^{n+1})}_{a_P^{n+1}\leftarrow} T_P^{n+1} &= \underbrace{(a_P^n - a_N^n)}_{a_P^n\leftarrow} T_P^n + a_E^n T_E^n + \\ &+ a_S^n T_S^n + a_W^n T_W^n + a_E^{n+1} T_E^{n+1} + \\ &+ a_S^{n+1} T_S^{n+1} + a_W^{n+1} T_W^{n+1} + \\ &+ \underbrace{S_u + 2T_n(a_N^n + a_N^{n+1})}_{S_u\leftarrow} \end{aligned} \tag{9}$$

After the above updates are performed, coefficients a_N^{n+1} and a_N^n are set to 0 in order to disregard the virtual neighbour. The same Dirichlet conditions apply to the western border of the reactor since the temperature is directly measured.

The energy losses through the bottom part of the reactor are neglected and this fact is translated into a Neumann border condition. The computations can be found in appendix A.3. The following coefficients updates were determined:

$$\begin{aligned} \underbrace{(a_P^{n+1} - a_E^{n+1})}_{a_P^{n+1}\leftarrow} T_P^{n+1} &= \underbrace{(a_P^n + a_E^n)}_{a_P^n\leftarrow} T_P^n + a_W^n T_W^n + a_S^n T_S^n \\ &+ a_N^n T_N^n + a_W^{n+1} T_W^{n+1} + a_S^{n+1} T_S^{n+1} + \\ &+ a_N^{n+1} T_N^{n+1} + \\ &+ \underbrace{S_u - \Delta x D_e(a_E^n + a_E^{n+1})}_{S_u\leftarrow} \end{aligned} \tag{10}$$

The same Neumann conditions are applied to the eastern border of the reactor, which is also considered perfect insulated. The types of boundary conditions have been summarized in figure 6.

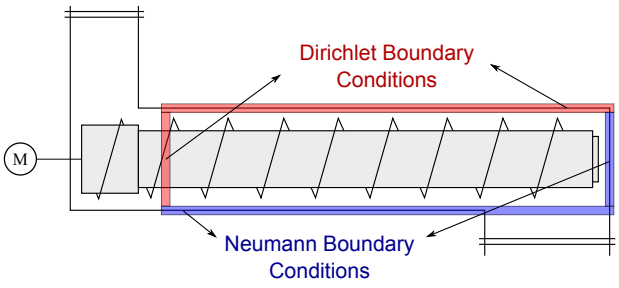

Fig. 6. Dirichlet and Neumann boundary conditions in the thermal reactor case.

An important thing to notice is the fact that, if coefficients (7) do not change in time, then the temperature model described by equation (6) becomes linear and the model can be formulated in a state space manner such that to facilitate fast simulation.

State Space Model In order to derive a state space model, the first step is to serialize and to assign a number to the control volumes from the thermal reactor grid as in figure 7. The first control volume is positioned in the lower left corner of the reactor and the last control volume $n_x n_y$ is situated in the top right corner where n_x and n_y are the dimensions of the grid.

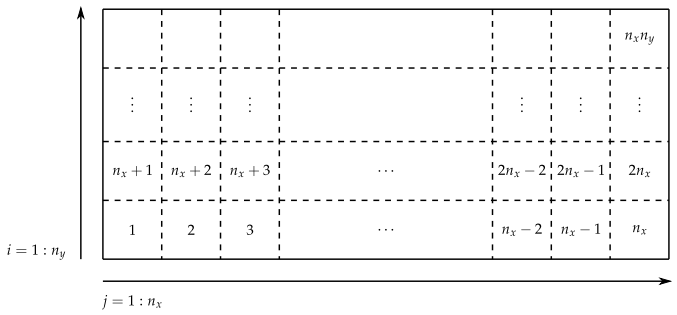

Fig. 7. The control volumes are assigned a number starting from the lowest left corner till the right top corner

Given the coordinates of a volume in the two dimensional space i.e. row i_c and column j_c then the corresponding index i_x in the state vector is found using the relation:

$$i_x = (i_c - 1)n_x + j_c \tag{11}$$

Since the model estimates temperatures, the hat notation will be used from now on to denote the temperature state vector. Let $\hat{x}_T$ comprise the temperatures in the sequentialized control volumes:

$$\begin{aligned} \hat{x}_T^n &= \begin{bmatrix} T_1^n & T_2^n & \cdots & T_{n_x}^n & \cdots & T_{n_x n_y}^n \end{bmatrix}^{\mathrm{T}} \\ \hat{x}_T^{n+1} &= \begin{bmatrix} T_1^{n+1} & T_2^{n+1} & \cdots & T_{n_x}^{n+1} & \cdots & T_{n_x n_y}^{n+1} \end{bmatrix}^{\mathrm{T}} \\ u_T^n &= \begin{bmatrix} S_{u_1}^n & S_{u_2}^n & \cdots & S_{u_{n_x}}^n & \cdots & S_{u_{n_x n_y}}^n \end{bmatrix}^{\mathrm{T}} \end{aligned} \tag{12}$$

where $\hat{x}_T^n$ is the state vector at time step n, $\hat{x}_T^{n+1}$ is the state vector at the next time step and u_T^n gathers all the source terms in the control volumes. Input vector u_T^n will be simplified later because not all of the control volumes have an input source term.

The state space model can be comprised in the following standard equation:

$$\mathbf{E_T}\hat{x}_T^{n+1} = \mathbf{A_T}\hat{x}_T^n + \mathbf{B_T}u_T^n \tag{13}$$

and can be reformulated as:

$$\begin{aligned} \hat{x}_T^{n+1} &= \underbrace{\mathbf{E_T^{-1}A_T}}_{\tilde{\mathbf{A}}_\mathbf{T}}\hat{x}_T^n + \underbrace{\mathbf{E_T^{-1}B_T}}_{\tilde{\mathbf{B}}_\mathbf{T}}u_T^n \\ \hat{x}_T^{n+1} &= \tilde{\mathbf{A}}_\mathbf{T}\hat{x}_T^n + \tilde{\mathbf{B}}_\mathbf{T}u_T^n \end{aligned} \tag{14}$$

where $\tilde{\mathbf{A}}_\mathbf{T}$ is the dynamic matrix and $\tilde{\mathbf{B}}_\mathbf{T}$ is the input matrix of the model.

Matrices $\mathbf{E_T}$, $\mathbf{A_T}$ and $\mathbf{B_T}$ have special structures and are determined by writing equation (6) for each control volume:

$$\mathbf{E_T} = \begin{bmatrix} a_{P_1}^{n+1} & -a_{E_1} & \cdots & \cdots & -a_{N_1} & 0 & \cdots & 0 \\ -a_{W_2} & a_{P_2}^{n+1} & -a_{E_2} & \cdots & 0 & -a_{N_2} & \cdots & 0 \\ \vdots & & & & & & & \\ 0 & & & & & & & \\ -a_{S_{nx+1}} & 0 & & & & & & \\ 0 & -a_{S_{nx+2}} & 0 & & & & & \\ \vdots & & & & & & & \end{bmatrix} \tag{15}$$

$$\mathbf{A_T} = \begin{bmatrix} a_{P_1}^n & a_{E_1} & 0 & \cdots & \cdots & a_{N_1} & 0 & 0 & \cdots & 0 \\ a_{W_2} & a_{P_2}^n & a_{E_2} & 0 & \cdots & 0 & a_{N_2} & 0 & \cdots & 0 \\ 0 & a_{W_3} & a_{P_3}^n & a_{E_3} & \cdots & 0 & 0 & a_{N_3} & \cdots & 0 \\ \vdots & & & & & & & & & \\ 0 & & & & & & & & & \\ a_{S_{nx+1}} & 0 & & & & & & & & \\ 0 & a_{S_{nx+2}} & 0 & & & & & & & \\ \vdots & & & & & & & & & \end{bmatrix} \tag{16}$$

The input matrix $\mathbf{B_T}$ is simplified by keeping only the relevant columns. The temperature of the steam layer is considered the first input into the model and its corresponding column in the $\mathbf{B_T}$ matrix is found from equation (9), where T_n is the input:

$$\mathbf{B_T}(:,1) = \begin{bmatrix} 0 & \ldots & 0 & 2D & 2D & \ldots & 2D \end{bmatrix}^{\mathrm{T}} \tag{17}$$

The temperatures of the western border are directly measured and constitute the remaining inputs:

$$\mathbf{B_T}(:,i) = \begin{bmatrix} 0 & \ldots & 0 & 2(D+F) & 0 & \ldots & 0 \end{bmatrix}^{\mathrm{T}} \tag{18}$$

where i is temperature sensor TI-21, TI-22, TI-23, TI-24 and TI-25. The non-zero coefficient from this column is selected with the help of equation (11) as the coordinates of the control volume where the sensor is positioned are known.

The output $\hat{y}_T^n$ of the system is defined as:

$$\hat{y}_T^n = \tilde{\mathbf{C}}_\mathbf{T}\hat{x}_T^n \tag{19}$$

where $\tilde{\mathbf{C}}_\mathbf{T}$ is the output matrix of the system and is set such to select the temperatures of the control volumes situated on the eastern border.

A system with 6 inputs i.e. TI-01, TI-21, TI-22, TI-23, TI-24 and TI-25 and 5 outputs i.e. TI-31, TI-32, TI-33, TI-34 and TI-35 is, therefore, obtained.

3.3 Kalman Filter

Because the system from equation (14) might be inaccurate when describing the temperature dynamics inside the reactor, a Kalman estimator would be appropriate. Missing dynamics might comprise the rotations of the snail, which contributes to the slurry mixing, gaps in the material where steam can be trapped and contributes to a non-uniform heating or the steam injection from the bottom, which heats the material as the steam travels to the top layer. A static Kalman gain $\tilde{\mathbf{K}}_\mathbf{T}$ is designed such that to ensure best fitting. This is achieved by formulating the state space model as a grey box model with an unknown state noise covariance matrix $\mathbf{R_v}$.

The real system may be written in the following state space formulation:

$$\begin{cases} x_T^{n+1} = \tilde{\mathbf{A}}_\mathbf{T} \cdot x_T^n + \tilde{\mathbf{B}}_\mathbf{T} \cdot u_n + \tilde{\mathbf{G}}_\mathbf{T} v_n \\ y_T^n = \tilde{\mathbf{C}}_\mathbf{T} \cdot x_T^n + e_n \end{cases} \tag{20}$$

where matrices $\tilde{\mathbf{A}}_\mathbf{T}$, $\tilde{\mathbf{B}}_\mathbf{T}$ and $\tilde{\mathbf{C}}_\mathbf{T}$ are defined as in (14) and $\tilde{\mathbf{G}}_\mathbf{T}$ is the state noise propagation matrix. Since all states represent temperatures, it is assumed that the noise is of the same type for all states. All control volumes are affected by its own noise sequence and when augmenting the system together, v_n becomes a column vector with

the same length as x_T^n. The noise vectors v_n and e_n are assumed to be normally distributed white sequences with 0 mean and $\mathbf{R_v}$ and, respectively, $\mathbf{R_e}$ covariance matrices:

$$\begin{cases} v_n \in \mathbf{N}(0, \mathbf{R_v}) \\ e_n \in \mathbf{N}(0, \mathbf{R_e}) \end{cases} \tag{21}$$

The derivation of matrix $\tilde{\mathbf{G}}_\mathbf{T}$ is performed by deviating the temperature variable T from the convection-diffusion equation (5) by a random amount v assumed to be normally distributed with 0 mean and variance R_v. It turns out that $\tilde{\mathbf{G}}_\mathbf{T} = \tilde{\mathbf{A}}_\mathbf{T}$, which is expected since the system was considered linear.

After the static Kalman gain is found, it is desired to bring the model to its innovation form:

$$\begin{cases} \hat{x}_T^{n+1} = \tilde{\mathbf{A}}_\mathbf{T} \cdot \hat{x}_T^n + \tilde{\mathbf{B}}_\mathbf{T} \cdot u_n + \tilde{\mathbf{K}}_\mathbf{T} \cdot e_T^n \\ \hat{y}_T^n = \tilde{\mathbf{C}}_\mathbf{T} \cdot \hat{x}_T^n + e_T^n \end{cases} \tag{22}$$

where e_T^n is the innovation defined as:

$$e_T^n = y_T^n - \tilde{\mathbf{C}}_\mathbf{T} \cdot \hat{x}_T^n \tag{23}$$

3.4 Model Estimation and Validation

Two pairs of input-output data are extracted from the logged sensor information presented in figure 3. One set is used for model estimation and the other one for validation. The grey-box estimation procedure is run and the below state noise variance is found:

$$r_v = 0.0037 \tag{24}$$

which corresponds to a variation of $\pm 0.1566\,^\circ\mathrm{C}$ (2.5758σ). Variance r_v is positioned on the main diagonal of the state noise covariance matrix $\mathbf{R_v}$.

The predicted outputs and the real sensor data are compared. Only the results for one output i.e. TI-35 are presented in figure 8 due to space considerations. The predicted output illustrated with a blue line stays within the yellow confidence interval as shown in the top two subplots. The innovations drawn in the bottom subplots look white and stay within the confidence interval most of the time, which proves that the Kalman filter has a good performance.

Good fitting results were also obtained in the case of the other outputs i.e. TI-34, TI-33, TI-32 and TI-31.

4. SENSOR MOUNTING

The model obtained in equation (22) is embedded into a temperature soft sensor and is connected to the current thermal reactor setup as in figure 9. The soft sensor requires information mainly from the temperature sensor stripes. If the horizontal speed is held constant then the system matrices also remain constant and can be computed offline resulting in a linear model. If the horizontal speed is changed then the system matrices have to be updated as the convection coefficient F needs to be recomputed every time step.

In a block diagram formulation, the temperature soft sensor is connected as in figure 10. The required signals and the outputs of the sensor are explicitly shown in this figure.

The temperature soft sensor provides $\hat{x}_T$, which describes the temperature distribution inside the reactor in a two dimensional space.

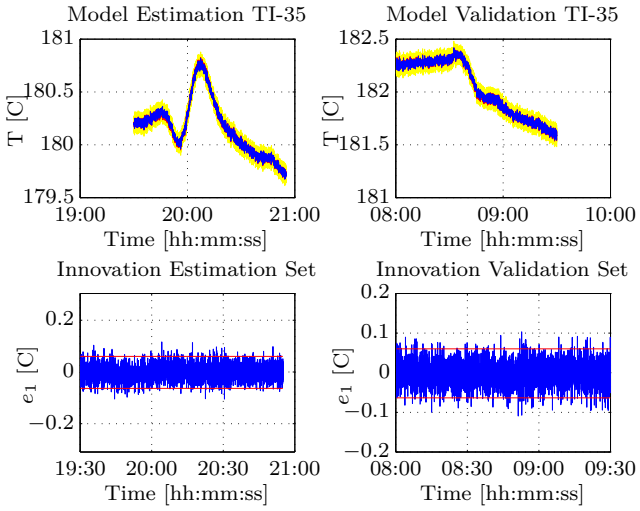

Fig. 8. Model validation TI-35. A fitting of 87% is achieved on both datasets. The top plots present the fitting results while the bottom plots show the innovation or the error estimation.

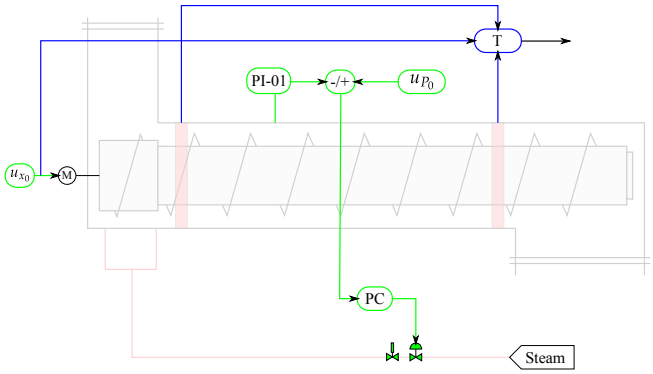

Fig. 9. Sensor mounting. The temperature soft sensor T requires information from the installed temperature measurements and from the nominal horizontal speed. The pressure control system is also illustrated.

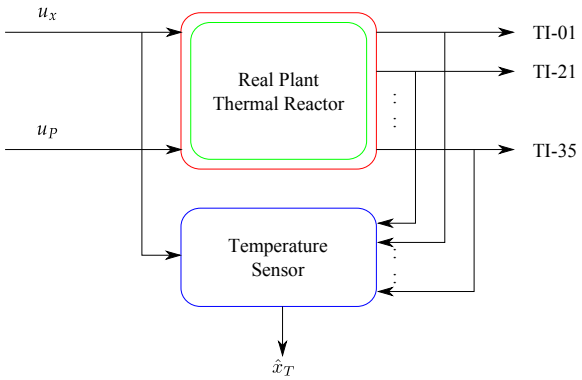

Fig. 10. Temperature sensor mounting block diagram.

5. SIMULATION RESULTS

The temperature soft sensor has been implemented defining a 60x5 grid i.e. 60 divisions on horizontal and 5 on vertical, resulting in an overall model with 300 states. A resolution of 5 divisions on vertical was preferred due to the existing 5 sensors distributed on the height of the reactor.

Real logged data is fed into the sensor and a snapshot is taken during the simulation. Figure 11 displays the temperature distribution constructed from $\hat{x}_T$ as isothermic lines. This figure proves that the temperature model is able to capture the temperature difference between the top and the bottom part of the thermal reactor in real time. As it was seen in figure 3, the temperature is subjected to sinusoidal disturbances. The disturbances are more severe in the upper part of the container and this is also visible in figure 11. The lower right corner of the reactor has an opening towards a downstream component, which acts like a cold source. This is why the temperature decreases as approaching the right ending of the reactor and the effect is well captured by the temperature soft sensor.

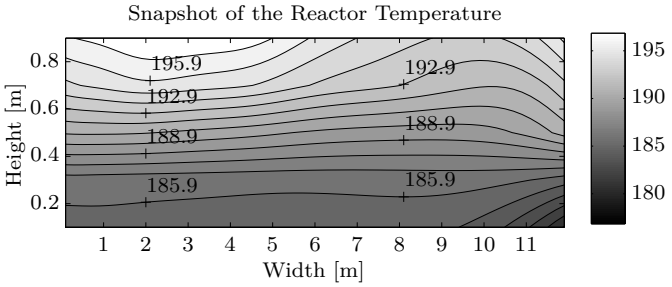

Fig. 11. Snapshot of isothermic lines.

The simulation was run assuming that the thermal reactor is fully filled with biomass, which is, in fact, wrong. There is no direct indication of the biomass level as it is difficult to measure but it could be determined based on the results from the new soft sensor. In figure 11 it is seen that the upper part of the tank changes temperature more rapidly than the lower half portion of the reactor, which rather remains almost constant. This is an indication that the internal environment does not have a constant density. Therefore, the level of biomass can be estimated and, in the current simulation case, a half filled reactor would explain the isothermic lines.

After estimating the level of biomass, the density and thermal conductivity of the control volumes not occupied by biomass can be changed and a more accurate result would be obtained.

6. CONCLUSIONS

A distributed model for the reactor temperature was successfully derived given an irregular environment characterized by temperature differences on both horizontal and vertical axes. The heat convection diffusion equation from computational fluid dynamics proved to give good results in describing the temperature gradient. The Kalman filter also proved to perform well and the obtained temperature gradient captures most of the effects that occur. The state space representation of the model was valuable for efficient simulations and can be further used for monitoring or control purposes.

The operator of the plant is now able to observe how the biomass is treated in any point of the reactor. The operator is also able to analyse the effects of the subsequent components on the reactor temperature, like the temperature drop that occurs near the opening end of the tank.

Valuable information can be obtained from the temperature gradient with respect to the efficiency of the current architecture of the thermal reactor. Ideally, the temperature inside the reactor should be the same in any point of the tank (a uniform environment). The plant operators are now able to observe how efficient the bottom inlets of steam can be and reconfiguration of the reactor can occur in order to achieve a temperature environment closer to the ideal one.

Appendix A. TEMPERATURE MODELLING

A.1 The Finite Volume Method

The key step of the finite volume method is to integrate equation (5) over the control volume:

$$\int_{\Delta V} \rho c \frac{\partial T}{\partial t} dV + \int_{\Delta V} \rho c u \frac{\partial T}{\partial x} dV = \int_{\Delta V} \frac{\partial}{\partial x}\left(\kappa \frac{\partial T}{\partial x}\right) dV + \\ + \int_{\Delta V} \frac{\partial}{\partial y}\left(\kappa \frac{\partial T}{\partial y}\right) dV + \int_{\Delta V} S_T dV \tag{A.1}$$

Using the divergence theorem (Egeland and Gravdahl, 2002, p. 403), the integrals containing partial derivatives with respect to x and y from equation (A.1) can be rewritten like below:

$$\int_{\Delta V} \rho c u \frac{\partial T}{\partial x} dV = \int_{\Delta V} \frac{\partial}{\partial x}\left(\rho c u T\right) dV = \int_{A} \mathbf{n}^{\mathrm{T}}\left(\rho c u T\right) dA \\ \int_{\Delta V} \frac{\partial}{\partial x}\left(\kappa \frac{\partial T}{\partial x}\right) dV = \int_{A} \mathbf{n}^{\mathrm{T}}\left(\kappa \frac{\partial T}{\partial x}\right) dA \\ \int_{\Delta V} \frac{\partial}{\partial y}\left(\kappa \frac{\partial T}{\partial y}\right) dV = \int_{A} \mathbf{n}^{\mathrm{T}}\left(\kappa \frac{\partial T}{\partial y}\right) dA \tag{A.2}$$

where $\mathbf{n}$ is a unit vector normal to the surface. The temperature in the control volume is assumed uniform and this allows the evaluation of integrals (A.2) at the east and west or south and north boundaries respectively:

$$\int_{A} \mathbf{n}^{\mathrm{T}}\left(\rho c u T\right) dA = \left(\rho c u A T\right)_e - \left(\rho c u A T\right)_w \\ \int_{A} \mathbf{n}^{\mathrm{T}}\left(\kappa \frac{\partial T}{\partial x}\right) dA = \left(\kappa A \frac{\partial T}{\partial x}\right)_e - \left(\kappa A \frac{\partial T}{\partial x}\right)_w \\ \int_{A} \mathbf{n}^{\mathrm{T}}\left(\kappa \frac{\partial T}{\partial y}\right) dA = \left(\kappa A \frac{\partial T}{\partial y}\right)_s - \left(\kappa A \frac{\partial T}{\partial x}\right)_n \tag{A.3}$$

The results from (A.3) are substituted into (A.2) and then into (A.1) and the following result yields:

$$\int_{\Delta V} \rho c \frac{\partial T}{\partial t} dV + \left(\rho c u A T\right)_e - \left(\rho c u A T\right)_w = \\ \left(\kappa A \frac{\partial T}{\partial x}\right)_e - \left(\kappa A \frac{\partial T}{\partial x}\right)_w + \\ + \left(\kappa A \frac{\partial T}{\partial y}\right)_s - \left(\kappa A \frac{\partial T}{\partial y}\right)_n + \bar{S}\Delta V \tag{A.4}$$

where the source term in a control volume is averaged as $\bar{S}$ and, therefore, considered constant inside the volume. The

partial derivative with respect to time is isolated on the left hand side of the equation:

$$\begin{aligned}\int_{\Delta V}\rho c\frac{\partial T}{\partial t}dV = \left(\kappa A\frac{\partial T}{\partial x}\right)_e - \left(\kappa A\frac{\partial T}{\partial x}\right)_w + \\ + \left(\kappa A\frac{\partial T}{\partial y}\right)_s - \left(\kappa A\frac{\partial T}{\partial y}\right)_n + \\ (\rho cuAT)_w - (\rho cuAT)_e + \bar{S}\Delta V\end{aligned} \tag{A.5}$$

Equation (A.5) tells that the accumulation in time of thermal energy is a result of three effects i.e. diffusion, convection and generated heat by the control volume itself. Diffusion occurs on horizontal and vertical, from west to east and from north to south respectively. Accumulation of energy is a balance between energy that enters the control volume plus generated energy minus the amount of energy that leaves the volume.

A.2 Discretization

Equation (A.5) is solved by integrating in time and then is discretized using a parameterized method θ:

$$\begin{aligned}\rho c\Delta V T_P^{n+1} = \rho c\Delta V T_P^n + \\ \Delta t\left[\theta f\left(T_P^n, n, x\right) + (1-\theta) f\left(T_P^{n+1}, n+1, x\right)\right]\end{aligned} \tag{A.6}$$

where f is a function that gathers all the terms on the right hand side of equation (A.5). The integration method depends on parameter θ. If $\theta = 1$ then, from equation (A.6), the temperature in control volume P at time step $n+1$ depends only on previous information from time step n. This procedure is also known as the explicit Euler or backward integration method and is equivalent to building a rectangle from time step n. Parameter θ can also be 0 and then the rectangle is built from step $n+1$ to step n or, in other words, the temperature in control volume P at time step $n+1$ depends only on information from time step $n+1$. When θ is 0, the procedure is also called the implicit Euler or forward integration method. A more accurate method is the Crank-Nicolson procedure, which relies on trapezoids instead of rectangles and it corresponds to $\theta = 1/2$.

Equation (A.6) is divided by the integration time Δt:

$$\begin{aligned}\rho c\frac{\Delta V}{\Delta t}T_P^{n+1} = \rho c\frac{\Delta V}{\Delta t}T_P^n + \\ \theta f\left(T_P^n, n, x\right) + (1-\theta) f\left(T_P^{n+1}, n+1, x\right)\end{aligned} \tag{A.7}$$

where $f\left(T_P^n, n, x\right)$ gathers all the variables from time step n. The partial derivatives from (A.5) can be approximated like in the following example:

$$\left.\frac{\partial T}{\partial x}\right|_e \approx \frac{T_E - T_P}{\delta x_{PE}} \tag{A.8}$$

where the partial derivative of temperature T with respect to x is evaluated at the east boundary of the control volume as the ratio between the difference of temperatures in the centers of the control volumes E and P and the distance between their centers δx_{PE}. By conducting these approximations, the following expression for $f\left(T_P^n, n, x\right)$ is found:

$$\begin{aligned}f\left(T_P^n, n, x\right) = \kappa_e A_e\frac{T_E^n - T_P^n}{\delta x_{PE}} - \kappa_w A_w\frac{T_P^n - T_W^n}{\delta x_{WP}} + \\ \kappa_s A_s\frac{T_S^n - T_P^n}{\delta x_{PS}} - \kappa_n A_n\frac{T_P^n - T_N^n}{\delta x_{NP}} + \\ +\rho cuA_w T_w^n - \rho cuA_e T_e^n + \bar{S}\Delta V\end{aligned} \tag{A.9}$$

The constant coefficients from (A.9) are grouped into:

$$\begin{cases} F_e = \rho cuA_e \\ F_w = \rho cuA_w \end{cases} \qquad \begin{cases} D_e = \dfrac{\kappa_e A_e}{\delta x_{PE}} \\ D_w = \dfrac{\kappa_w A_w}{\delta x_{WP}} \\ D_n = \dfrac{\kappa_n A_n}{\delta x_{NP}} \\ D_s = \dfrac{\kappa_s A_s}{\delta x_{PS}} \end{cases} \tag{A.10}$$

where F is also known as the convection term and D is called the diffusion term.

Two more temperatures remain to be evaluated i.e. the temperature at the east boundary T_e and the temperature at the west boundary T_w. The flow direction is known as being from west to east. It was assumed in the introduction section of this chapter based on the real data that there is not a lot of heat diffusion and the convection part has a higher effect. In such cases, it is recommended to use the upwind difference scheme (UDS), which considers the temperatures at the east and west boundaries T_e and T_w as:

$$T_e = T_P \qquad T_w = T_W \tag{A.11}$$

The choice of the difference scheme can be quantized by the use of the Peclet number, which defines the transportiveness and is a measure of the ratio between convection and diffusion:

$$P_e = \frac{F}{D} \tag{A.12}$$

If the Peclet number P_e is greater than 2 then the convection effect is more prominent and an UDS scheme is more appropriate. If $P_e < 2$ then heat diffusion is more important and another approximation scheme is recommended (Bingham et al., 2010) i.e. the central difference scheme (CDS).

The source quantity of volume P from (A.9) can vary in time and it would be preferred to linearize it around T_P^n:

$$\bar{S}\Delta V = S_u + S_P T_P^n \tag{A.13}$$

and then equation (A.9) becomes:

$$\begin{aligned}f\left(T_P^n, n, x\right) = D_e\left(T_E^n - T_P^n\right) - \\ -D_w\left(T_P^n - T_W^n\right) + D_s\left(T_S^n - T_P^n\right) - D_n\left(T_P^n - T_N^n\right) + \\ +F_w T_W^n - F_e T_P^n + S_u + S_P T_P^n\end{aligned} \tag{A.14}$$

$$\begin{aligned}f\left(T_P^n, n, x\right) = \left(S_P - D_e - D_w - D_s - D_n - F_e\right) T_P^n + \\ +D_e T_E^n + (D_w + F_w) T_W^n + \\ +D_s T_S^n + D_n T_N^n + S_u\end{aligned} \tag{A.15}$$

Function f is also evaluated at time step $n+1$:

$$f\left(T_P^{n+1}, n+1, x\right) = D_e\left(T_E^{n+1} - T_P^{n+1}\right) - \\ -D_w\left(T_P^{n+1} - T_W^{n+1}\right) + \\ +D_s\left(T_S^{n+1} - T_P^{n+1}\right) - D_n\left(T_P^{n+1} - T_N^{n+1}\right) + \\ +F_w T_W^{n+1} - F_e T_P^{n+1} + S_u + S_P T_P^{n+1} \\ f\left(T_P^{n+1}, n+1, x\right) = \\ = \left(S_P - D_e - D_w - D_s - D_n - F_e\right) T_P^{n+1} + \\ +D_e T_E^{n+1} + (D_w + F_w) T_W^{n+1} + D_s T_S^{n+1} + D_n T_N^{n+1} + S_u \tag{A.16}$$

(A.17)

The expressions of function f at time steps n and $n+1$ are substituted into equation (A.7) and all constant coefficients are grouped as below:

$$\begin{aligned} a_P^{n+1} T_P^{n+1} &= a_P^n T_P^n + a_E^n T_E^n + a_W^n T_W^n + a_S^n T_S^n + a_N^n T_N^n + \\ &+ a_E^{n+1} T_E^{n+1} + a_W^{n+1} T_W^{n+1} + a_S^{n+1} T_S^{n+1} + \\ &+ a_N^{n+1} T_N^{n+1} + S_u \end{aligned} \tag{A.18}$$

Coefficients a_P^n, a_E^n, a_W^n, a_S^n, a_N^n and a_P^{n+1}, a_E^{n+1}, a_W^{n+1}, a_S^{n+1}, a_N^{n+1} are detailed next:

$$\begin{aligned} a_P^n &= \rho c \frac{\Delta V}{\Delta t} - \theta\left(D_e + D_w + D_s + D_n + F_e - S_P\right) \\ a_E^n &= \theta D_e \\ a_W^n &= \theta\left(D_w + F_w\right) \\ a_S^n &= \theta D_s \\ a_N^n &= \theta D_n \end{aligned} \tag{A.19}$$

$$\begin{aligned} a_P^{n+1} &= \rho c \frac{\Delta V}{\Delta t} + \\ &+ (1-\theta)\left(D_e + D_w + D_s + D_n + F_e - S_P\right) \\ a_E^{n+1} &= (1-\theta) D_e \\ a_W^{n+1} &= (1-\theta)\left(D_w + F_w\right) \\ a_S^{n+1} &= (1-\theta) D_s \\ a_N^{n+1} &= (1-\theta) D_n \end{aligned} \tag{A.20}$$

If coefficients (A.19) and (A.20) remain constant in time then the temperature model described by equation (A.18) is linear.

A.3 Boundary Conditions

The boundary conditions are set as suggested by (Bingham et al., 2010) and will be explained next. There are two types of boundary conditions depending on whether the temperature is considered known at the border or the temperature gradient or energy loss is estimated at the border. When the temperature is set to a value, the boundary condition is also called a Dirichlet condition. Figure 5 illustrates the Dirichlet setup for a general grid where the boundary condition is notated as T_i where i is one of the borders east e, west w, south s or north n.

In the case of the thermal reactor, the temperature on the northern boundary is directly measured with 3 sensors and is considered constant and known on the x axes. This is the indication of a steam layer that is formed on the top part of the reactor. A virtual or auxiliary control volume is created at the boundary with a temperature T_{a_N} that has to be determined such that at the boundary a temperature T_n or T north is reached. A linear interpolation is used between the temperature from the centers of the auxiliary a_N volume and current P volume:

$$T(y) = T_n + \frac{T_P - T_{a_N}}{\Delta y} y \tag{A.21}$$

where $T(y)$ is the temperature along the y axes, T_n is the temperature at the northern border, T_P is the temperature in the control volume P, T_{a_N} is the temperature of the auxiliary control volume and Δy is the distance between P and a_N. Temperature $T(y)$ is evaluated at the center of the auxiliary volume considering that the y axes has its origin at the northern border and pointing downward:

$$T\left(-\frac{\Delta y}{2}\right) = T_{a_N} \Rightarrow \\ T_{a_N} = T_n - \frac{T_P - T_{a_N}}{\Delta y}\frac{\Delta y}{2} = T_n - \frac{T_P - T_{a_N}}{2} \tag{A.22}$$

from where the center temperature of the auxiliary control volume T_{a_N} is found:

$$T_{a_N} = T_n + \frac{T_{a_N}}{2} - \frac{T_P}{2} \Rightarrow \\ \frac{T_{a_N}}{2} = T_n - \frac{T_P}{2} \Rightarrow T_{a_N} = 2T_n - T_P \tag{A.23}$$

Equation (A.18) is evaluated for the control volumes that have a known temperature at the boundaries considering the auxiliary control volumes. In the case of a northern auxiliary neighbor equation (A.18) becomes:

$$a_P^{n+1} T_P^{n+1} = a_P^n T_P^n + a_E^n T_E^n + a_N^n (2T_n - T_P^n) + \\ +a_S^n T_S^n + a_W^n T_W^n + a_E^{n+1} T_E^{n+1} + \\ a_N^{n+1}(2T_n - T_P^{n+1}) + a_S^{n+1} T_S^{n+1} + a_W^{n+1} T_W^{n+1} + S_u \tag{A.24}$$

The source term and the coefficients of T_P^{n+1} and T_P^n of the control volumes subjected to the boundary conditions change as below:

$$\underbrace{\left(a_P^{n+1} + a_N^{n+1}\right)}_{a_P^{n+1}\leftarrow} T_P^{n+1} = \underbrace{\left(a_P^n - a_N^n\right)}_{a_P^n\leftarrow} T_P^n + a_E^n T_E^n + \\ + a_S^n T_S^n + a_W^n T_W^n + a_E^{n+1} T_E^{n+1} + \\ + a_S^{n+1} T_S^{n+1} + a_W^{n+1} T_W^{n+1} + \\ + \underbrace{S_u + 2T_n\left(a_N^n + a_N^{n+1}\right)}_{S_u\leftarrow} \tag{A.25}$$

It is important to set a_N^{n+1} and a_N^n to 0 after the previously indicated updates have been performed in order to disregard the auxiliary control volume.

The same Dirichlet boundary conditions are applied on the western boundary of the reactor. Remember from the process description chapter that there are several sensors i.e. TI-1211621, TI-1211622, TI-1211623, TI-1211624 and TI-1211625 positioned on the y axes at the beginning of the reactor. The temperature inside the reactor will be

modeled starting from this position onward and, therefore, these sensors constitute the western boundary conditions.

If the tank is insulated then the partial derivative of the temperature with respect to the x or y axes is considered null. If there are losses of heat energy due to insulation then this derivative may have a non-zero value. The reactor is considered perfect insulated at all of its borders although one might include the opening towards the hydrocyclone as a loss of energy. It will be later shown that this energy loss can be neglected. Boundary conditions with known temperature derivatives are also called Neumann type conditions and are illustrated in the same figure 5 where the derivatives D_n, D_w, D_e and D_s are positioned at the borders.

An auxiliary control volume is created just as in the Dirchlet case (Bingham et al., 2010) but this time, the derivative at the border is known and approximated as:

$$D_e \approx \frac{T_P - T_a}{\Delta x} \Rightarrow T_{a_E} = T_P - \Delta x D_e \tag{A.26}$$

where D_e is the derivative at the eastern border considered as an example to illustrate the procedure. The temperature of the auxiliary control volume is then easily found as in (A.26). Equation (A.18) is then reevaluated at the eastern boundary:

$$\begin{aligned} a_P^{n+1}T_P^{n+1} = {} & a_P^n T_P^n + a_E^n(T_P^n - \Delta x D_e) + a_W^n T_W^n + \\ & + a_S^n T_S^n + a_N^n T_N^n + \\ & + a_E^{n+1}(T_P^{n+1} - \Delta x D_e) + a_W^{n+1}T_W^{n+1} + \\ & + a_S^{n+1}T_S^{n+1} + a_N^{n+1}T_N^{n+1} + S_u \end{aligned} \tag{A.27}$$

The source term and the coefficients of T_P^{n+1} and T_P^n are updated as below:

$$\begin{aligned} \underbrace{(a_P^{n+1} - a_E^{n+1})}_{a_P^{n+1}\leftarrow} T_P^{n+1} = {} & \underbrace{(a_P^n + a_E^n)}_{a_P^n\leftarrow} T_P^n + a_W^n T_W^n + a_S^n T_S^n \\ & + a_N^n T_N^n + a_W^{n+1}T_W^{n+1} + a_S^{n+1}T_S^{n+1} + \\ & + a_N^{n+1}T_N^{n+1} + \\ & + \underbrace{S_u - \Delta x D_e(a_E^n + a_E^{n+1})}_{S_u\leftarrow} \end{aligned} \tag{A.28}$$

Again, it is important not to forget to set a_E^n and a_E^{n+1} to 0 in order to disregard the auxiliary point. Following the example for the eastern boundary, the southern border can be processed. Notice that, if the derivative is considered null as in this case, the source term does not need to be updated.

REFERENCES

Bingham, H.B., Larsen, P.S., and Barker, A.V. (2010). *Computational Fluid Dynamics*. DTU.

Datta, R., Maher, M.A., Jonesc, C., and Brinkerd, R.W. (2011). Ethanol - the primary renewable liquid fuel. *Journal of Chemical Technology & Biotechnology*, 86, 473–480.

Egeland, O. and Gravdahl, J.T. (2002). *Modeling and Simulation for Automatic Control*.

Kristensen, J.B., Thygesen, L.G., Felby, C., Jørgensen, H., and Elder, T. (2008). Cell-wall structural changes in wheat straw pretreated for bioethanol production. *Biotechnology for Biofuels*.

Larsen, J., Petersen, M.Ø., Thirup, L., Li, H.W., and Iversen, F.K. (2008). The ibus process - lignocellulosic bioethanol close to a commercial reality. *Chemical Engineering & Technology*, 31, 765–772.

Overend, R.P., Chornet, E., and Gascoigne, J.A. (1987). Fractionation of lignocellulosics by steam-aqueous pretreatments. *Phil. Trans. R. Soc. Lond. A*, 321, 523–536.

Petersen, M.Ø., Larsen, J., and Thomsen, M.H. (2009). Optimization of hydrothermal pretreatment of wheat straw for production of bioethanol at low water consumption without addition of chemicals. *Biomass and Energy*, 33, 834–840.

Thomsen, M.H., Thygesen, A., and Thomsen, A.B. (2009). Identification and characterization of fermentation inhibitors formed during hydrothermal treatment and following ssf of wheat straw. *Biotechnological Products and Process Engineering*, 83, 447–455.